國 立 交 通 大 學

電子工程學系電子研究所

碩 士 論 文

利用通道背向散射理論對遠距庫倫散射遷移率之研究

Analysis of Remote Coulomb Scattering Mobility Using Channel Backscattering Theory

研 究 生：湯侑穎

指導教授：陳明哲　教授

中 華 民 國 九 十 八 年 九 月

利用通道背向散射理論對遠距庫倫散射遷移率之研究

Analysis of Remote Coulomb Scattering Mobility Using Channel Backscattering Theory

研 究 生：湯侑穎　　Student: Yu-Ying Tang

指導教授：陳明哲　　Advisor: Min-Jer Chen

國 立 交 通 大 學

電子工程學系　電子研究所

碩 士 論 文

A Thesis

Submitted to Department of Electronics Engineering & Institute of Electronics

College of Electrical and Computer Engineering

National Chiao Tung University

in Partial Fulfillment of the requirements

for the Degree of Master

in

Electronic Engineering

September 2009

Hsinchu, Taiwan, Republic of China

中華民國九十八年九月

利用通道背向散射理論對遠距庫散射遷移率之研究

研究生：湯侑穎　　指導教授:陳明哲博士

國立交通大學

電子工程學系電子研究所

摘要

近來許多研究指出，當氧化層厚度小於 2~3 奈米時，等效電子遷移率會隨著氧化層厚度的減少而減少。研究認為等效電子遷移率的減少是因多晶矽閘極中的遠距電荷所產生的遠距庫倫散射所導致。利用通道背向散射理論以及建立在三角位能井理論基礎上的模擬器，我們可以從Fischetti的蒙地卡羅模擬結果中得到平均自由徑 λ。透過不同情況下的等效電子速度所推得的不同平均自由徑 λ，可以從中分析出由多晶矽閘極空乏區中的電荷所造成的遠距庫倫散射造成的平均自由徑 λ 變化量，並由此經通道背向散射理論計算得遠距庫倫散射電子遷移率。這個方法提供了一個簡單的新方式可以估算遠距庫倫散射電子遷移率 μ_{rcs}，其結果與其他相關研究比較，亦合理且接近。

Analysis of Remote Coulomb Scattering Mobility Using Channel Backscattering Theory

Student: Yu-Ying Tang Advisor: Dr. Ming-Jer Chen

Department of Electronics Engineering

Institute of Electronics

National Chiao Tung University

Abstract

Many investigations point out that when the thickness of oxide layer is less than 2~3nm, the effective electron mobility will be degraded with the reduction of gate oxide thickness. It is suggested that the mobility degradation of ultrathin gate oxide devices may be caused by the Coulomb scattering from remote charge in the poly gate. Using the channel backscattering theory and triangular potential approximation simulator TRP, an important parameter mean free path λ can be fitted to the Fischetti's Monte Carlo data. After fitting the mean-free-path λ from effective electron velocity in the different cases, we can distinguish the fraction of λ caused by the remote charge scattering due to the charge in the depletion region of the poly gate and calculate the remote charge scattering mobility μ_{rcs} with λ_{rcs} through the backscattering theory. This new method can therefore offer a simple way to estimate Coulomb scattering mobility μ_{rcs}; and the results have been corroborated proved through the comparison with the recent experiment date.

誌　謝

在此感謝陳明哲老師，在我就讀碩士班期間的悉心指導以及提供良好的研究環境與資源；並以嚴謹的態度，以身作則的為我們樹立做研究的典範。感謝已早一步畢業的謝振宇學長，還有博士班的李建志、許智育、李韋漢學長，他們總是不厭其煩的在我的碩士班生活上提供各方面的協助與指導。也謝謝陳又正與陳以東兩位同學在求學生涯的陪伴及激勵，一起度過了很多在實驗室趕進度挑燈夜戰的時光。實驗室的學弟妹也在平常提供了不少協助，並帶給實驗室很多活力與歡樂。特別要感謝詹益先學弟，在一起合作的研究中展現了過人的能力以及研究上的幫助。最後要感謝我的父母及妹妹，還有女朋友謝佩芸，作為我的後盾以及支柱，讓我能無後顧之憂的完成碩士學業。

2009 年 9 月

湯侑穎

Contents

List of Captions

Chapter 1

Introduction

With the development of IC technology, the feature length of metal-oxide-semiconductor field effect transistors (MOSFETs) has been scale down to less than 100nm in the resent years. And it has also been predicted that the feature length of MOSFETs will further scale down to 22nm in the next generation devices. However, when the feature length shrinks until a few nanometers, the conventional classically-based carrier transport model, such as drift-diffusion model, would lose its accuracy in nanoscale devices. In order to deal with this issue, channel backscattering theory constructed by Mark Lundstrom [1],[2] can serve as a key tool to research the carrier transport in nanoscale devices. The main merits of backscattering theory are that (1) it can provide a clear understanding of the underlying device physics, on the basis of a small fraction of the channel near the quasi-equilibrium source, rather than the traditional high-field near the drain; (2) it can meet the computationally efficient requirement; and (3) it can furnish information about how close to the thermal limit the device performance can achieve.

On the other hand, with the decreasing of the gate oxide thickness, the scattering caused by the charge in the depletion region of the poly gate of the MOSFET will decrease the mobility [3]. This scattering effect is named remote Coulomb scattering (RCS) or remote charge scattering. Remote Coulomb scattering shows a strong effect on electron mobility

reduction when oxide layer is thinner than 2nm [3],[4],[5],[6].

In this thesis, we try to link backscattering theory to the remote Coulomb scattering. With finding of the best fitting of the mean free path λ in different cases from Monte Carlo simulation [7],[8], we can calculate the remote Coulomb scattering mobility μ_{rcs}. In Chapter 2, we will introduce the backscattering theory and a triangular potential approximation model, which will be used in the calculations of this component. In Chapter 3, we will show the introduction of remote Coulomb scattering and the Monte Carlo simulation in different cases. Chapter 4 will show how we fit the mean free path λ and calculate the remote Coulomb scattering mobility μrcs. Results is comparison with the data elsewhere [3] is shown in Chapter 4. Finally, we will make a short conclusion in the chapter 5.

Chapter 2

Triangular Potential Approximation and Backscattering Theory

2-1 Triangular Potential Approximation and Quantum Mechanical Calculation

In this work, we use a simulator developed by our group, which is based on the triangular approximation of the electron potential well [9]. Triangular potential approximation can offer accurate results about the behaviors of electrons in the channel. With this approximation taken into account, we have an inversion carrier density per subband as

$$N_{ij} = \left(\frac{n_{vi} m_{di} k_B T}{\pi \hbar^2} \right) \ln\left(1 + \exp\left(\frac{E_F - E_{ij}}{k_B T} \right) \right) \quad (2\text{-}1)$$

Where i=1,2 (valley) , j=1,2,3 (subband)….; nv is the degeneracy of i-th valley; and mdi is the density of states effective mass of the i-th valley. EF is the quasi-Fermi level while Eij is the energy level of i-th valley and j-th subband, as expressed below

$$E_{ij} = \left(\frac{\hbar^2}{2 m_{zi}} \right)^{1/3} \left(\frac{3}{2} q \pi F_{Si} \left(j - \frac{1}{4} \right) \right)^{2/3} \quad (2\text{-}2)$$

The total inversion layer charge per area is given by $N_{inv} = \sum N_{ij}$. With known E_{ij}, the total inversion layer thickness can be expressed as

$$Z_{ij} = \frac{2\varepsilon_{si} E_{ij}}{3q\varepsilon_{ox} F_{ox}} \quad (2\text{-}3)$$

Here F_{ox} is oxide electric field and $F_{ox} = V_{ox} / t_{ox}$. Then we can get the average inversion layer thickness:

$$Z_{QM} = \sum \frac{Z_{ij} N_{ij}}{N_s} \quad (2\text{-}4)$$

Potential drop of depletion drop V_{dep} can be written as

$$V_{depl} = Vs - \frac{qNsZ_{QM}}{\varepsilon_{si}} - \frac{k_B T}{q} \quad (2\text{-}5)$$

where V_s is the band bending in the substrate.

$$V_s = |V_G - V_{FB}| - V_{poly} - V_{ox} \quad (2\text{-}6)$$

Here V_{FB} is the total flat-band voltage, V_{poly} is potential drop due to the poly gate depletion and V_{ox} is voltage drop across the oxide.

Ionized impurity density per area can be expressed as

$$N_{depl} = \sqrt{\frac{2\varepsilon_{si} V_{depl} N_{sub}}{q}} \quad (2\text{-}7)$$

With subband levels and Fermi level, the effective thermal injection velocity at the top of the potential barrier can be expressed as [2],[10]

$$\upsilon_{inj}^{j} = \sqrt{\frac{2k_B T m_{ci}}{\pi m_{di}^2} \left(\frac{\Im_{1/2}(\eta_F)}{\ln\left(1 + e^{\eta_F}\right)} \right)} \quad (2\text{-}8)$$

where $\Im_{1/2}(\eta_F) = \frac{1}{\Gamma\left(\frac{3}{2}\right)} \int_0^\infty \frac{\eta^{1/2} d\eta}{1+e^{\eta-\eta_F}} = \frac{2}{\sqrt{\pi}} \int_0^\infty \frac{\eta^{1/2} d\eta}{1+e^{\eta-\eta_F}}$ (2-9)

and $\eta_F = \frac{E_F - E_i}{k_B T}$

Here m_{ci} is the conductivity effective mass of i-th subband and m_{di} is the density of states effective mass for i-th subband. With triangle potential approximation, we can simplify the calculation task in our work.

2-2 Backscattering Theory

Channel backscattering theory [1],[2] assumes the carrier transport in the channel is a wave-like flux traveling from source to drain. In this theory, k_B-T layer is the key region which controls the flux ratio passing through the channel, where k_B is Boltzmann's constant and T is the temperature. As shown in Fig.2-1, k_B-T layer represents the region from the top of the channel potential to the point where the potential drops around the by thermal energy of k_BT/q, and this distance is named *l*. r_c is the channel backscattering coefficient. Multiple backscattering events occur in this critical region, and this region determines the current at the drain, as shown below

$$I_D = Q_{inv} \upsilon_{inj} \frac{1-r_c}{1+r_c} \quad (2\text{-}10)$$

Q_{inv} is the inversion layer charge density per unit area at the top of the potential barrier, which is also the location of the virtual source, and Q_{inv} appropriately follows the MOS electrostatics: $Q_{inv}=C_{eff}(V_G-V_{th})$. Here C_{eff}

is the inversion gate capacitor per unit area and V_{th} is the threshold voltage. υ_{inj} is thermal injection velocity at the top virtual source or virtual source. Parameter r_c is the channel backscattering coefficient, standing for the fraction of the injecting flux F reflected and returning to the source while $(1-r_c)$ standing for the fraction of the injected flux transmitting to the drain. The r_c vary is from 0 to 1. Backscattering theory also links r_c to both the quasi-thermal-equilibrium mean-free-path λ for backscattering and the critical length of k_B-T layer *l*, as expressed below

$$r_c = \frac{1}{1+\frac{\lambda}{l}} \quad (2\text{-}11)$$

The range of r_c is from 0 to 1.

2-3 Compact Models for the Critical Length *l*

On the basis of a parabolic potential profile around the source-channel junction barrier of nanoscale MOSFETs, a new compact model has been physically derived elsewhere [11], which links the width of thermal energy k_B-T layer to the geometrical and bias parameters of the device:

$$l = \eta L \frac{V_D^{0.25}}{(V_G - V_{th})^{0.5}} \frac{1}{V_D^{0.25}} \frac{k_B T}{q} \quad (2\text{-}12)$$

Here η is fixed and also is the only fitting parameter. It is expected that η is a constant, regardless of the channel length, gate and drain voltage, and temperature; otherwise, the applicability of the resulting model may be

limited. In the citation [11], through fitting with other experimental and Monte Carlo simulation results, *l* versus the quantity of the functional expression, as shown in Fig.2-2

$$LV_D^{0.25}(V_G - V_{th})^{-0.5}\left(\frac{k_B T}{q}\right)^{0.5}\left(\frac{k_B T}{qV_D}\right)^{0.5} \quad (2\text{-}13)$$

In the figure, η is the value of 4.1($V^{-0.25}$). As expected, η remains constant, regardless of the channel length, gate and drain voltage, and temperature. As the result, the critical length *l* can be expressed as

$$l = 4.1L\frac{V_D^{0.25}}{(V_G - V_{th})^{0.5}}\left(\frac{k_B T}{q}\right)^{0.5}\left(\frac{k_B T}{qV_D}\right)^{0.5} \quad (2\text{-}14)$$

Here $V_{th} = V_{th0} - V_D * DIBL$. V_{th0} can be extracted from a plot of inversion layer charge versus gate voltage at low drain voltage bias. DIBL is "Drain Induced Barrier Lowering", which can be reasonably adjusted by throughout the work

.

2-4 Injection Velocity and r_c Calculation Using Simulator TRP

In the simulator developed by our group, which named TRP, one of the important calculation methods is implemented as below:

$$N = \frac{1}{2}(1+r_c)n^+\left(1+\left(\frac{1-r_c}{1+r_c}\right)\frac{\left(\log\left(1+\exp\left(\frac{E_{frc}-E_{irc}-qV_D}{k_BT}\right)\right)\right)}{\left(\log\left(1+\exp\left(\frac{E_{Frc}-E_{irc}}{k_BT}\right)\right)\right)}\right) \quad (2\text{-}15)$$

where N represents N_{inv} at equilibrium state [12] and n^+ is new N_{inv} at E_{frc} and E_{irc}. In the program, we guess E_{frc} and E_{irc} with an initial value, then change E_{frc} and E_{irc} until (2-15) is satisfied in a loop. In this way, a set of new E_{frc} and E_{irc} can be determined and take into account the effect of r_c . Injection velocity with r_c can also be calculated through (2-8) and (2-9) with known E_{frc} and E_{irc}. Results of injection velocity from r_c=0 to r_c=1 are shown in Fig.2-3.In the figure, the injection velocity decreases with increasing of r_c.

Chapter 3

On Remote Coulomb Scattering

3-1. Remote Coulomb Scattering

As the feature length of MOSFETs is aggressively scaled, the thickness of oxide layer is also scaled simultaneously. Many investigations point out that when the thickness of oxide layer is less than 2~3nm, the effective electron mobility will be degraded with the reduction of gate oxide thickness. It is suggested that the mobility degradation of ultrathin gate oxide devices may be caused by the Coulomb scattering from remote charge in the poly-crystalline silicon gate (poly-gate) [3],[4],[5],[6].

Fig.3-1 shows the band structure diagram of poly-Si/gate oxide/p-substrate at a positive gate bias. The ionized doping impurity atoms in the poly-gate depletion layer cause the changed impurity charge. These impurity charges give rise to Coulomb interactions, thus making the redistribution of the electrons in the inversion layer. Note that the redistribution of electrons in the inversion layer will cause the doping impurity charges to be screened as well [7].

On the other hand, in the short channel devices, the long-range source/drain-channel Coulomb interactions do not subtract momentum directly from the electron gas, but indirectly increase the

momentum-dissipation process. However, the gate-channel interactions can directly make a transfer of the momentum from the elections in the channel to the electrons in the gate. Thus it is expected to depress the channel effective electron velocity [7],[8].

3-2. Comparison with Monte Carlo Simulation

Fig.3-2 shows the Monte Carlo simulation results of effective electron velocity υ_{eff} in [7],[8]. In the simulation, the channel length and oxide thickness of the devices are scaled linearly from L=100nm/tox=5.6nm to L=11.8nm/tox=0.7nm. Substrate doping Nsub is doped from 1E17cm^{-3} to 8E17cm^{-3} with the scaling down. The poly-Si gate doping level is fixed at 1E20cm^{-3}. All parameters are shown in Table.3-1. The simulation is biased at V_D=V_G=1V. Three different comparisons have been made. "Full Coulomb effect" includes interactions in the source/drain-channel and gate-channel due to the remote Coulomb scattering. "Metal gate" has only Coulomb interactions in source/drain-channel but ignoring the Coulomb drag across the gate insulator. "No Coulomb effect" suppresses all Coulomb interactions and plasma oscillations. The result shows the effective electron velocity gm/Cg (here gm is transconductance per unit width and Cg is the capacitance per unit area of gate) versus the metallurgical channel length. From Fig.3-1, the effective electron velocity appears to increase as the channel length decreases until the channel length goes down to around 25~40nm. When the channel is shorter than 40nm, the effective electron velocity does not increase with decreasing channel length. This is because

of the increased momentum dissipation as the channel length decreases in the presence if the Coulomb interactions.

It is very interesting to examine the change of the conditions effective election velocity under different Coulomb interactions, specially linking the effective electron velocity with backscattering theory.

Chapter 4

Remote Coulomb Mobility Parameter Extraction

4-1. Mean Free Path λ

In our study, we try to fit mean-free-path λ, an important parameter in backscattering theory, to the Fischetti's MC data [7],[8] achieved by means of the triangular potential approximation simulator and the backscattering theory. After fitting the mean-free-path λ from effective electron velocity in the different cases, we can distinguish the fraction of λ caused by the remote charge scattering due to the charge in the depletion region of the poly gate and calculate the remote charge scattering mobility μ_{rcs} with λ_{rcs} through the backscattering theory:

$$\upsilon_{eff} = \upsilon_{inj}\frac{1-r_c}{1+r_c} \quad (4\text{-}1)$$

$$r_c = \frac{1}{1+\frac{\lambda}{l}} \quad (4\text{-}2)$$

Here the injection velocity υ_{inj} is also a function of r_c. When r_c changes from 0 to 1, the change of υ_{inj} is only about 11~17% in different devices. It means that r_c is the main parameter which can mainly determine υ_{eff} in (4-1). The critical length *l* is derived from (2-14). We can adjust λ to change r_c and υ_{eff}, so that the effective electron velocity in Fig.3-2 can

be best fitted. With this method on the bases of backscattering theory and triangular potential approximation simulator, we can straight forwardly examine the remote Coulomb scattering effect.

Case I: No Coulomb Effect

In the simulation of "No Coulomb effect", there are not any Coulomb interactions in source/drain region or gate region. We tried different length of mean-free-path λ_1 at L=11.8, 25, 50, and 100nm under DIBL=0, 100, and 200 mV/V, and found the best fitted λ_1. The fitting results are shown in Fig.4-1.

Case II: Metal Gate

"Metal gate" means that it does not contain gate-channel interactions but contains interactions between source/drain and channel in the simulation. Here, we assume that the Coulomb interactions between source/drain and channel do not make any change in the mean-free-path λ_1. Instead, these interactions between source/drain and channel affect the potential along the channel, which in turn results in the change in the critical length *l*. With this in mind, we can use the mean-free-path λ_1, which is fitted from "No Coulomb effect" as known parameters. Then we can fit another set of critical length *l'* from the effective electron velocity of "Metal gate". The fitting results are shown in Fig.4-2(a). Here we assume that the difference between critical length in "No Coulomb effect" *l* and critical length in "Metal gate" *l'* would be the form of "times". In other words *l'*=A**l*. The results of "times" A are shown in Fig.4-2(b).

Case III: Full Coulomb Effect

"Full Coulomb effect" includes remote charge interactions both in source/drain-channel and gate-channel. On the other hand, not only critical length *l* but also mean-free-path λ are affected by Coulomb interactions. Here we use the same critical length *l'* fitted from "Metal gate" because in these two cases, Coulomb interactions in source/drain-channel cause the same effect on the both cases. Then we can fit new mean-free-path λ_2 from effective electron velocity in case of "Full Coulomb effect". The fitting results are shown in Fig.4-3

4-2. Remote Coulomb Scattering Mobility

After analysis of the difference between "Metal gate" and "Full Coulomb effect", it can be argued that "Full Coulomb effect" contains the Coulomb drag across the gate insulator but "Metal gate" does not. This difference corresponds to the difference between the mean free path λ of "Metal gate" and "Full Coulomb effect". The difference of the λ_1 and λ_2 is due to the fraction caused by gate remote Coulomb scattering due to the impurity charge in the depletion layer of poly-gate. In other words, we can express the relationships as follows [1],

$$\frac{1}{\mu_{all}} = \sum_i \frac{1}{\mu_i} \quad (4\text{-}3)$$

$$\lambda_{rcs} = \frac{2\mu_{rcs} k_B T}{q\upsilon_{inj}} \quad (4\text{-}4)$$

$$\frac{1}{\lambda_2} - \frac{1}{\lambda_1} = \frac{1}{\lambda_{rcs}} \quad (4\text{-}5)$$

With these relationships incorporated, we can calculate the gate remote

Coulomb scattering mobility μ_{rcs}:

$$\mu_{rcs} = \frac{q\lambda_{rcs}\upsilon_{inj}}{2k_B T} \quad (4\text{-}6)$$

Fig.4-5 shows the results and the comparison with [3]. The results and the trend are quite the same with each other. Notice that we cannot get μ_{rcs} at tox=5.6nm. The reason is that tox=5.6nm is too thick so that the gate-channel remote Coulomb effect almost vanished [13].

Chapter 5

Conclusion

Remote Coulomb scattering is not ignorable when the thickness of oxide in MOSFET is less than 3~4nm. Effective electron mobility and effective electron velocity are both degraded with the reduction of oxide layer thickness. Many works have been done on this issue. With the backscattering theory, an important parameter in terms of the mean free path λ can be fitted from the effective electron velocity under different remote Coulomb effects. The fitting result can be used to calculate the remote Coulomb scattering mobility μ_{rcs}. This new method can therefore offer a simple way to estimate Coulomb scattering mobility μ_{rcs}; and the results have been corroborated proved through the comparison with the recent experiment date. Some investigator has noticed that backscattering theory will be a powerful tool in research of remote Coulomb effect in ultra-short channel devices [14].

References

[1] M. S. Lundstrom, “Elementary physics theory of the Si MOSFETs” IEEE Electron Device Letters, vol.18, pp.361-363, 1997.

[2] M. S. Lundstrom and Z. Ren, “Essential physics of carrier transport in nano scale MOSFETs” IEEE Trans. Electron Devices, vol.49, pp.133-141, 2002.

[3] M. S. Krishnan, Y. C. Yeo, Q. Lu, T. J. King, J. Bokor, and C. Hu, “Remote charge scattering in MOSFETs with ultra-thin gate dielectrics” IEEE Int. Electron Device Meeting, pp.571-574, 1998.

[4] S. Takagi and M. Takayanagi, “Experimental evidence of inversion-layer mobility lowering in ultrathin gate oxide metal-oxide-semiconductor field-effect-transistors with direct tunneling current” Journal of Applied Physics, vol.41, pp.2348-2352, part.1, no.4B, 2002.

[5] M. S. Krishnan, L. Chang, T. J. King, J. Bokor, and C. Hu, “MOSFETs with 9 to 13 A thick gate oxides” IEEE Int. Electron Device Meeting, pp.241-244 1999.

[6] N. Yang, W. K. Henson, J. R. Hauser, and J. J. Wortman, “Estimation of the effects of romote charge scattering on electron mobility of n-MOSFET’s with ultrathin gate oxides” IEEE Transactions on Electron Devices, vol.47, no.2, 2000.

[7] M. V. Fischetti and S. E. Laux, “Long-range Coulomb interactions in small Si device Part I. Performance and

reliability" Journal of Applied Physics, vol.89, no.2, 2001.

[8] M. V. Fischetti, T. P. O'R, S. Narayanan, C. Sache, S. Jin, J, J. Kim, and Y. Zan, "Theoretical study of some physical aspects of electronic transport in nMOSFETs at the 10-nm gate-length" IEEE Transactions on Electron Devices, vol.54, no.9, 2007.

[9] H. H. Mueller and M. J. Schulz, "Simplified method to calculate the band bending and subband energies in MOS capacitors", IEEE Trans. Electron Device, vol. 44, no.9, pp.1539-1543, 1997.

[10] S. M. Sze and Kwok K. Ng, "Physics of semiconductor devices third edition" Wiley-Interscience, 2007.

[11] M. J. Chen, and L. F. Lu, "A parabolic potential barrier-oriented compact model for the k_BT layer's width in nano-MOSFETs", IEEE Trans. Electron Devices, vol.55, no.5, pp.1265-1268, 2008.

[12] A. Rahman and M. S. Lundstrom, "A compact scattering model for the nanoscale double-gate MOSFET", IEEE Transactions on Electron Devices, vol.49, no.3, 2002.

[13] F. Gamiz and M. V. Fischetti, "Remote Coulomb scattering in metal-gate-semiconductor field effect transistors: Screening by electrons in the gate" Appl. Phys. Letters, Vol.83, no.23, pp.4848-4850, 2003.

[14] M. V. Fischetti, S. Jin, Tw. Tang, P. Asbeck, Y. Taur, S.E. Laux, and N. Sano, "Scaling MOSFETs to 10 nm: Coulomb effects, source starvation, and virtual source" Computational Electronics, 2009, IWCE '09, 13th International Workshop on.

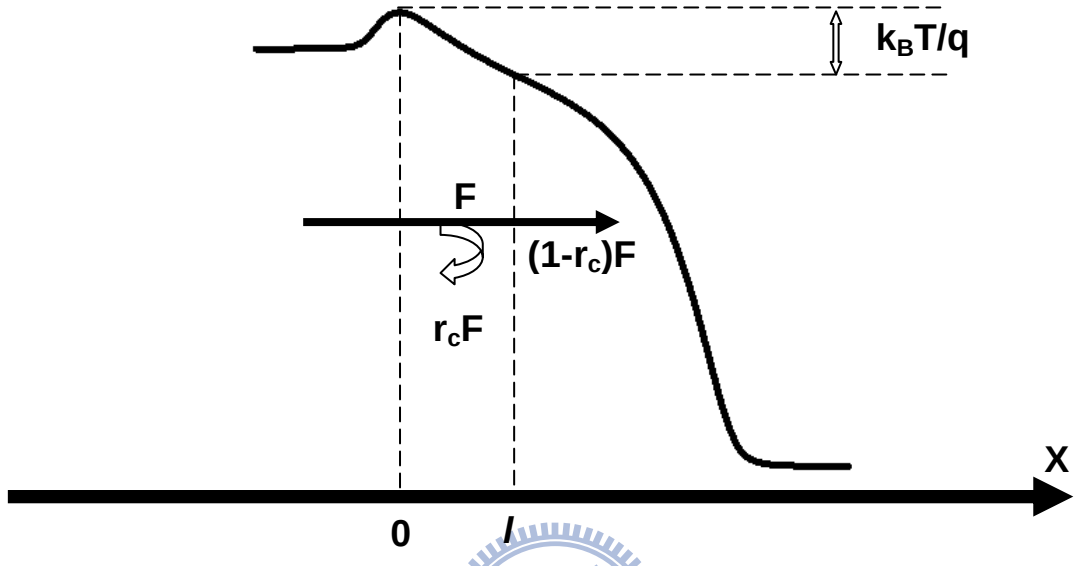

Fig.2-1 Schematic diagram of backscattering theory.

F is the incident flux from the source. *l* is the distance from the top of the barrier to the point where the potential drop is k_BT/q. r_c is the channel backscattering coefficient.

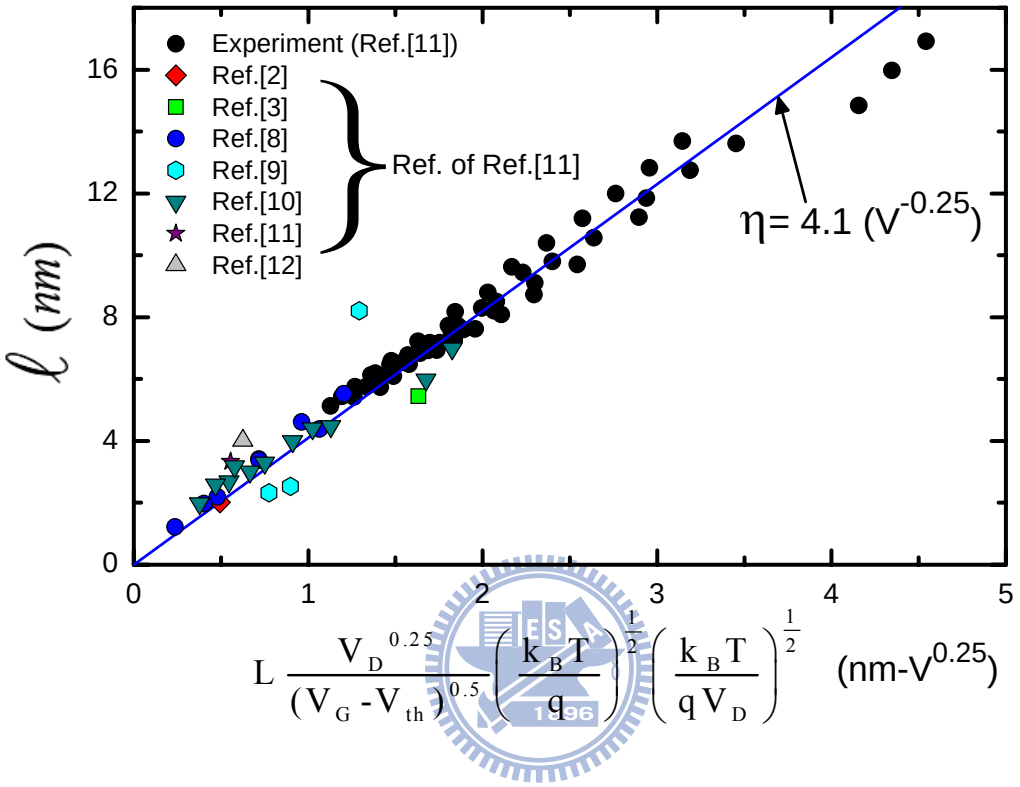

Fig.2-2 Scatter plot of the experimental and simulated *l* versus the quantity of the functional expression $LV_D^{0.25}(V_G - V_{th})^{-0.5}\left(\frac{k_BT}{q}\right)^{0.5}\left(\frac{k_BT}{qV_D}\right)^{0.5}$ **(nm-V$^{0.25}$). A straight line fits the data point. The slop of the line yields η of 4.1 V$^{-0.25}$.**

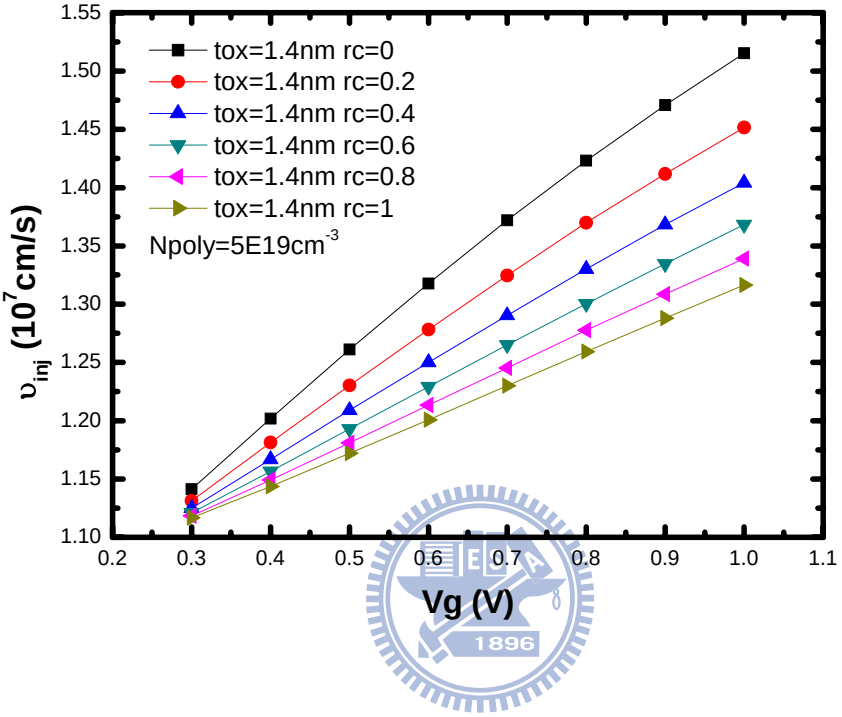

Fig.2-3 Injection velocity from r_c=0 to r_c=1. V_G=0~1V and V_D=1V for tox=1.4nm and Npoly=5E19cm^{-3}. Injection velocity decreases with increasing r_c.

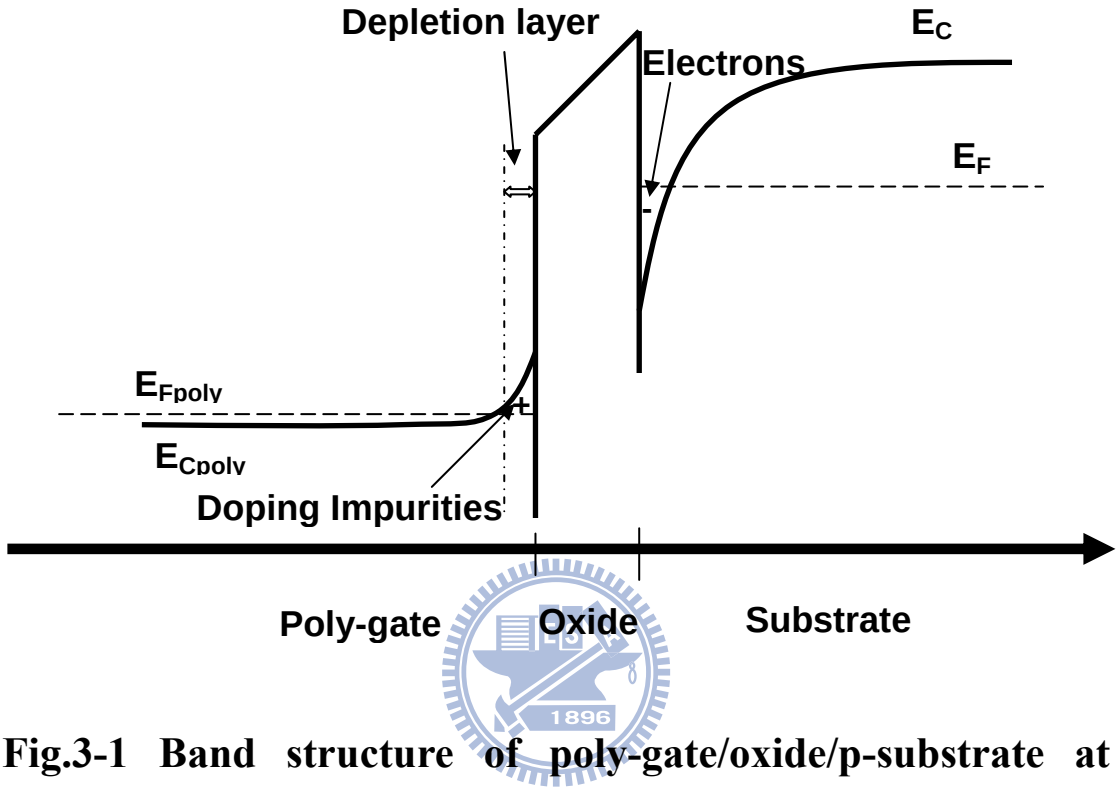

Fig.3-1 Band structure of poly-gate/oxide/p-substrate at positive gate bias.

L(nm)	100	50	25	11.8
t_{ox}(nm)	5.6	2.8	1.4	0.7
$N_{poly}(cm^{-3})$	5E19	5E19	5E19	5E19
$N_{sub}(cm^{-3})$	1E17	2E17	4E17	8E17
V_{th0}(V)	0.258	0.218	0.189	0.171

Table.3-1 Parameters of devices in the Monte Carlo simulation.

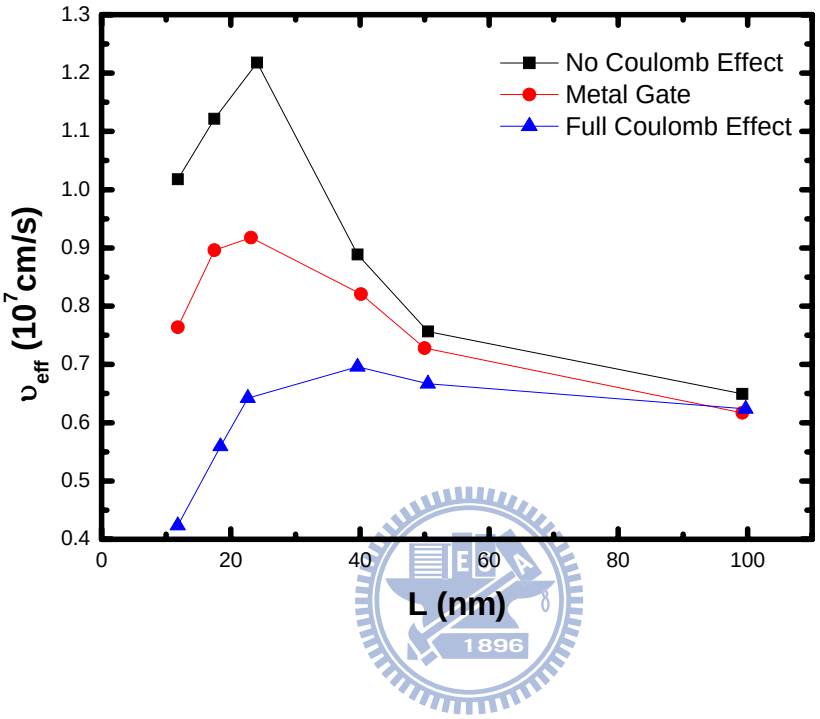

Fig.3-2 Results of Effective electron velocity from Monte Carlo Simulation.

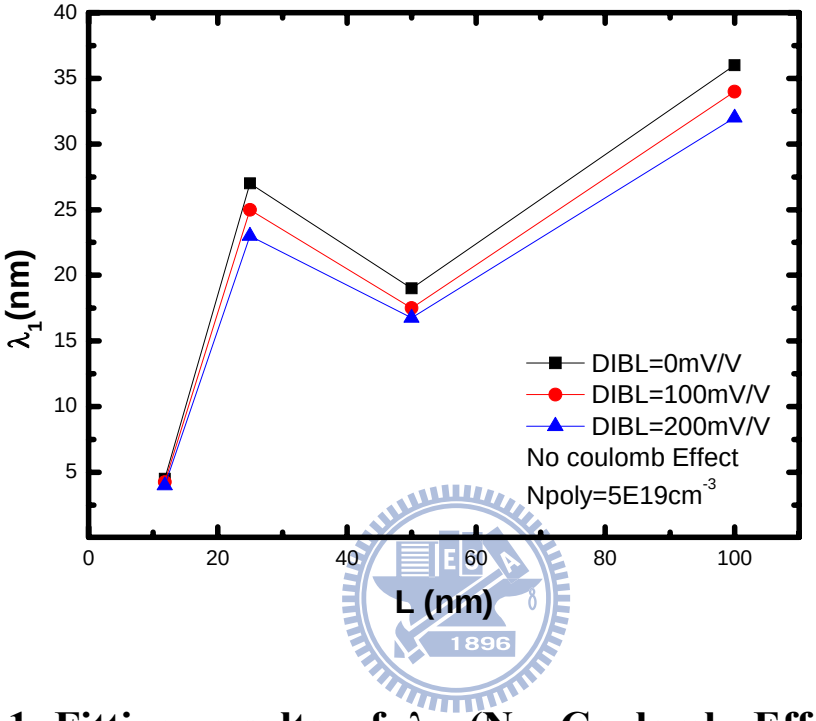

Fig.4-1 Fitting results of λ_1 (No Coulomb Effect) under DIBL=0, 100, and 200 mV/V.

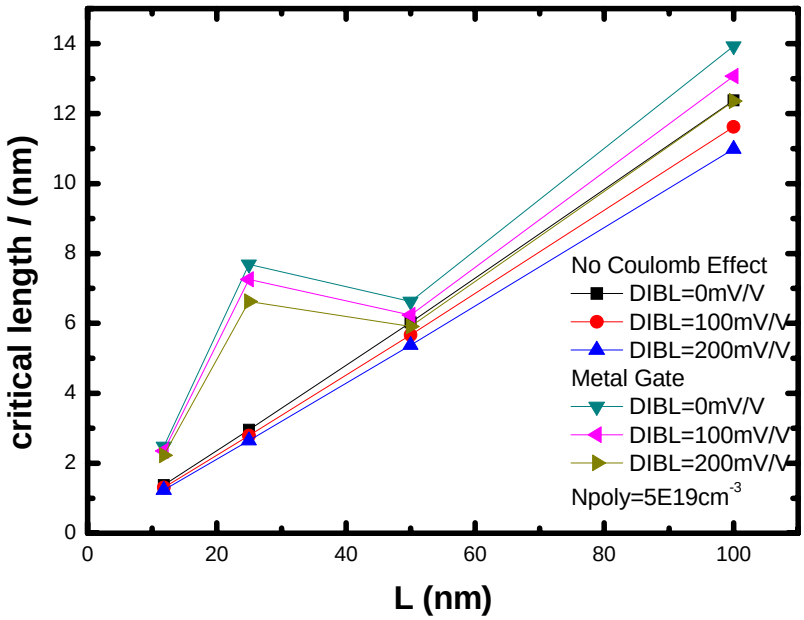

(a)

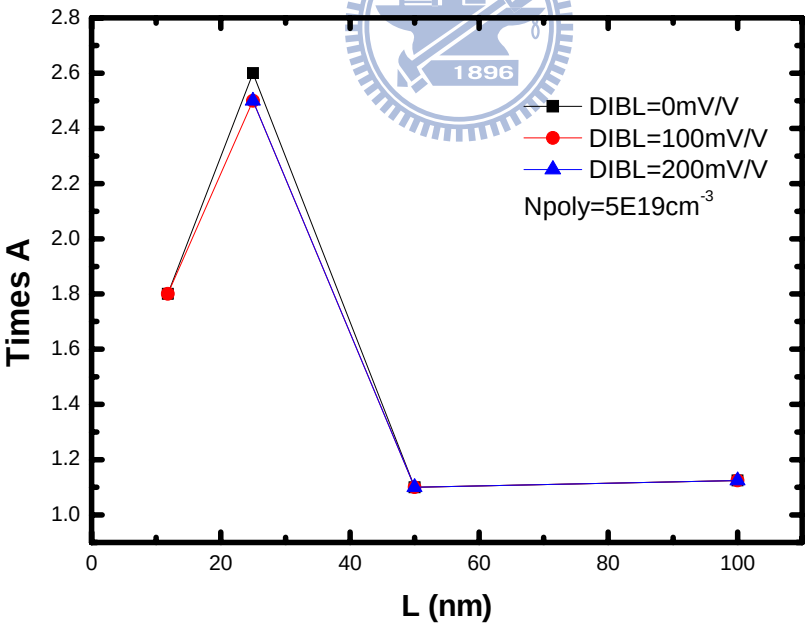

(b)

Fig.4-2 (a) Fitting result of *l* of (No Coulomb Effect) and *l'* (Metal Gate). (b) The Times A of *l* (*l'*/*l*)

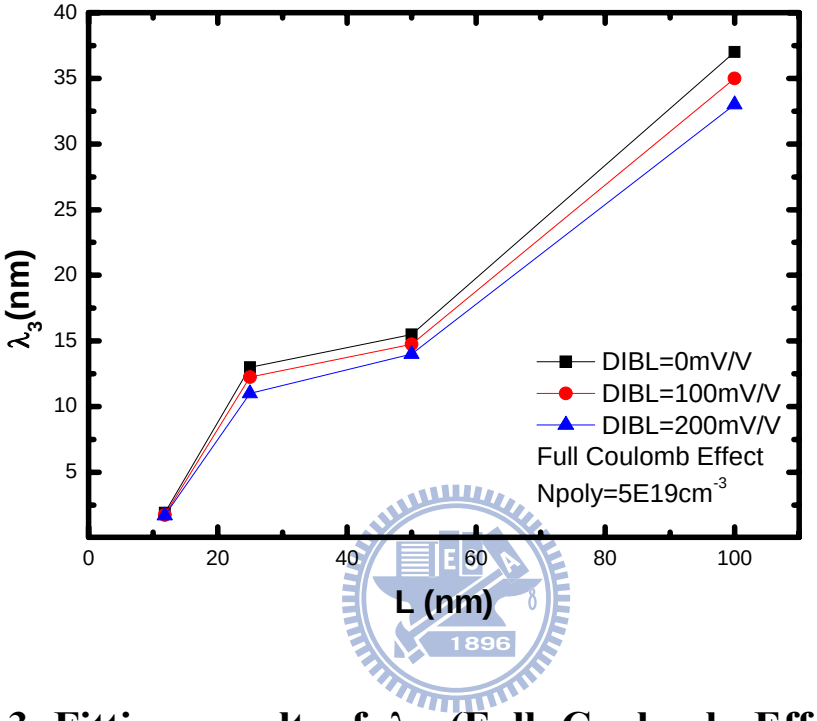

Fig.4-3 Fitting result of λ_3 (Full Coulomb Effect) under DIBL=0, 100, and 200 mV/V

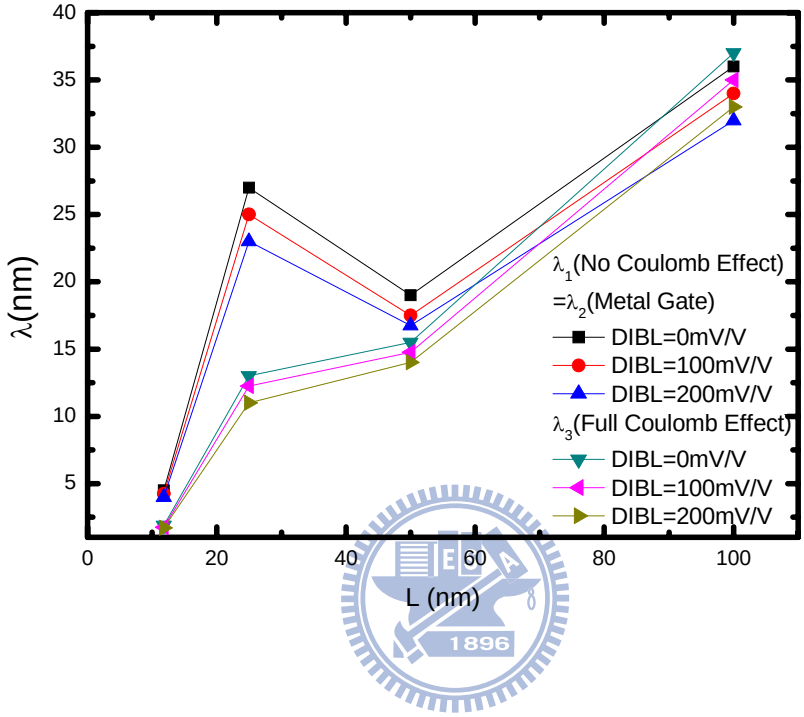

Fig.4-4 Comparison of mean free path λ of "No Coulomb Effect", "Metal Gate", "Full Coulomb Effect"

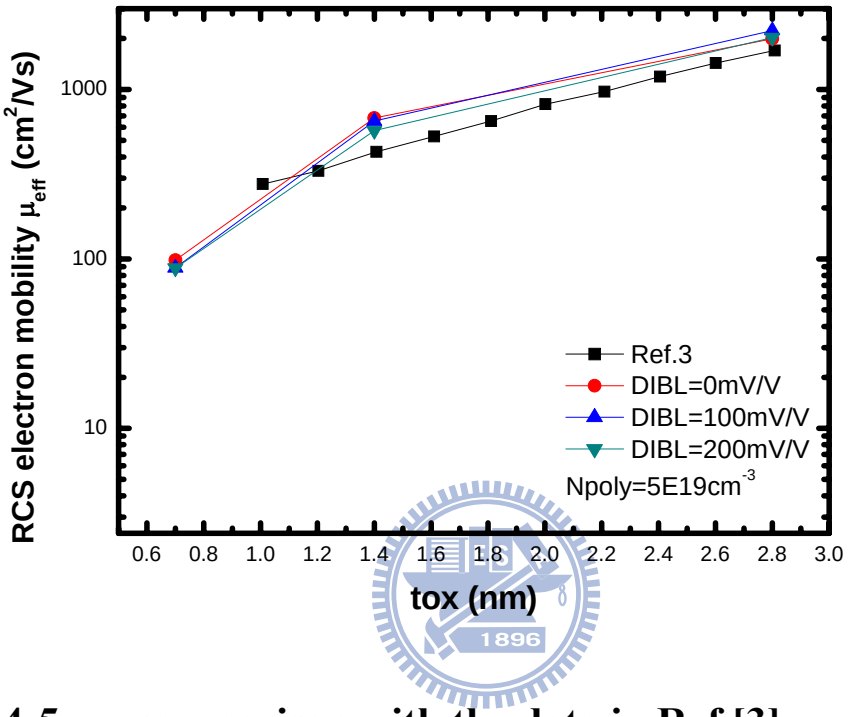

Fig.4-5 μ_{eff} comparison with the data in Ref.[3].